Jet noise reduction by impinging microjets: an aerodynamic investigation testing microjet parameters

T. Castelain*, M. Sunyach†, D. Juvé‡,

Ecole Centrale de Lyon, Laboratoire de Mécanique des Fluides et d'Acoustique, CNRS UMR 5509, Université Claude Bernard Lyon I, France

and J.-C. Béra†

INSERM U556, Université Claude Bernard Lyon I, Lyon, France

The effects of microjets on the aerodynamic characteristics of a Mach 0.9 high-Reynolds axisymmetric jet are investigated and are interpreted in the light of previous acoustic results. These measurements are obtained by means of Stereoscopic Particle Image Velocimetry in planes normal to the jet axis. Three parameters of the microjets system are varied: the outgoing mass flux per microjet, the number of microjets and their layout in the azimuth of the main jet. The aerodynamic results indicate a strong correlation between the maximum level of turbulence just behind the nozzle exit and the high-frequency noise, previously shown to potentially balance the acoustic benefits obtained for lower frequencies. The maximum level of turbulence measured at the longitudinal position corresponding to half the potential core length is also highly correlated to the jet noise reduction, which is highlighted by the similar evolution of these two quantities regarding the mass flux per microjet and the number of microjets. For low values of the number of microjets, the microjets are shown to act independently, and their contributions to the turbulence reduction are retrieved far downstream the impinging point without any noticeable azimuthal diffusion.

I. Introduction

Considering the growth of airplane traffic during the last few years, jet noise reduction remains a crucial stake. Such a reduction has already been obtained by passive systems, like tabs or chevrons (Simonich *et al.*,[1] Zaman,[2] and Zaman[3]), to the detriment of a thrust reduction affecting airplane performances. As an alternative, a micro-injection system impacting the main jet has been suggested, and resulted in a turbulence level reduction in part or full jet mixing layer (Arakeri *et al.*,[4] Alkislar *et al.*[5]), leading to jet noise reduction. Comparisons between the different microjets system implied in the above studies reveal that characteristic parameters of the control system, such as the flow at the microjet exit, the number of microjets and their diameters, could be quite different from one study to another. To define the influence of microjets configurations, Castelain *et al.*[6] previously reported the effects on the acoustic far-field of a microjets system whose geometrical and aerodynamical parameters have been varied. The present study focuses on the modification of the main jet flow field by microjets, and a parametric study based on Castelain *et al.*[6] was realized to interpret the far-field noise modification as a result of the turbulence reduction.

*PhD, AIAA Student Member, Mailing adress : Centre Acoustique, Ecole Centrale de Lyon, 36, avenue Guy de Collongue, 69134 Ecully Cédex, France. E-mail:thomas.castelain@gmail.com

†Professor, same address

‡Professor, AIAA Senior member, same address

II. Experimental set-up

A. Jet facility

The experiments were carried out in the anechoic facility of the Centre Acoustique, LMFA - École Centrale de Lyon. The jet, of diameter $D = 50$ mm, is powered by a centrifugal compressor of 450 kW with a maximum mass-flux of 1 kg.s^{-1}. After compression, the air was electrically heated by a set of resistances with a total power of 80 kW, to maintain the temperature of the expanded jet close to room temperature. This study focuses on a jet at a Mach number based on the ambiant speed of sound c_0 of $M_j = 0.9$, which corresponds to the jet Mach number used in the acoustic study made in the same facility.[6]

B. Microjets set-up

The control system is made of up to 36 microjets directed toward the jet centerline and impacting the jet with a 0° yaw angle. Previous studies[6,7] indicate that noise reduction due to microjets is sensitive to the geometrical parameters of the microjet system, and that a maximum noise reduction can be obtained by setting the microjets parameters, illustrated in Figure 1, to appropriate values. In this study, the microjet diameter d is 1 mm, the impinging angle α is 45°, the longitudinal distance l between the main jet nozzle lip and the microjet impact on the jet mixing layer is about 5% of the main jet diameter D.
The microjets are fed by a piston compressor, connected to a pressure reducer and pressure distributors. In order to impose a given mass flux through the microjets, the static pressure is monitored in each distributor with a 0-60PSI Honeywell XCA460an pressure sensor.
The mass flux per microjet (considered here in terms of its ratio r_m with the main jet mass flux), the number n and the azimuthal distribution of the microjets are decisive parameters regarding noise reduction. Moreover, considering recent results,[8] the distribution of n microjets in the azimuthal direction is also a parameter of interest. The parameter n can be varied from 3 to 36, respecting or not an axisymmetric arrangement of the microjets.

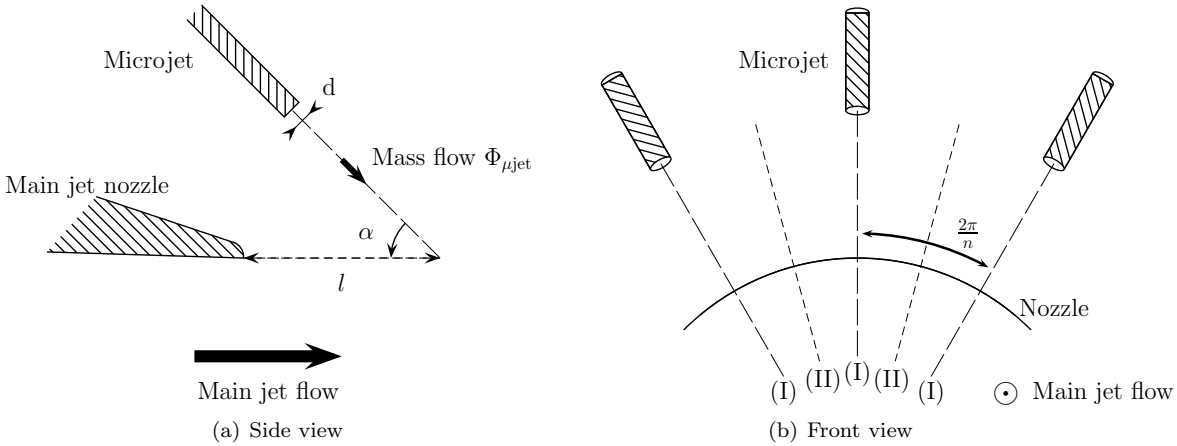

(a) Side view (b) Front view

Figure 1. Schematic of the microjets impinging the jet mixing layer. Illustration of some geometrical and aeraulical parameters of the microjet system and description of the typical radius orientations (I or II) used in Figure 2.

C. Flow field measurements

Data acquisition

The flow field measurements are obtained by Stereoscopic Particle Image Velocimetry (SPIV). To account for the inhomogeneity of the flow in the azimuthal direction due to the microjets impact on the jet mixing layer, the plane of interest is normal to the jet axis. A double pulsed Nd:YaG laser (NewWave Solo PIV III, 50 mJ) is used to form a 2mm-width light sheet in the measurement plane. The time between two consecutive pulses is set so that the maximum displacement of the particule in the potential core is one-third of the lightsheet thickness, to avoid out-of-plane errors in data processing.[9]

The jet is seeded by oil droplets generated by Laskin nozzles[10] operating 40D upstream the nozzle exit. Recirculation of the flow in the anechoic facility, far downstream the nozzle exit, and additionnal smoke particles obtained with a SAFEX Nebelgerät fog generator are used to ensure the seeding of the air entrained by the jet.

Two PCO SensiCam cameras, with CCD sensors corresponding to 1280×1024 px^2, are positionned on either side of the jet axis, and are combined with two AF Micro 60mm Nikkor ($f/2.8$) lenses. The angle between the optical axes of the two lenses is 90°, and the optical arrangement is symmetrical with respect to the x axis to minimize the errors in measurements.[9] Each camera image plane is rotated so that the Scheimpflug criterion is satisfied, permitting off-axis imaging with a sharp focus in the whole field of view.

POST-PROCESSING

Sets of the two pairs of images are processed with the LaVision 7.1.1 software, by the use of a multipass algorithm[11] with a final interrogation window size of 16×16 pixels and a zero-overlap between the interrogation area. Before the computational step of the estimation of the displacement, self-calibration on particle images is applied to account for any slight misalignement between the calibration plate and the LASER sheet.[12] The spatial resolution of the velocity fields corresponds roughly to 2% of the jet diameter D. Turbulence statistics are built on 1000 instantaneous velocity fields, derived from 1000 pairs of images pairs, as two cameras are used for these SPIV measurements.

III. Results

A. Mean flow field analysis

The mean flow field is described by the use of the Stereoscopic PIV measurements, made in transversal planes located every $1D$ from the longitudinal position $x/D = 1$ to $x/D = 7$. Characteristics of the mean flow field, like the azimuthal vorticity whose an approximation is given in Figure 2 with the radial derivative of the axial velocity, are described by an azimuthal averaging of the in-plane measurements. In this section, the microjets system is composed of 18 microjets with a mass flux per microjet ratio $r_m$of 2.7 10^{-4}. The microjets are axisymmetrically distributed around the nozzle exit. To account for the azimuthal inhomogeneity induced by the impingement of the microjets, the azimuthal averaging is based on radii separated of $\pi/9$ in the azimuthal direction, considering the geometry of the microjets system. As reported in Figure 2, at the early stages of the jet development and typically for $x/D = 1$, the radial distribution of the mean azimuthal vorticity is greatly modified by the control and lowered downstream the microjet impingement (profile I), and is essentially lowered between two consecutive microjet impingements (profile II). These results are fully consistent with Arakeri[4] and Alkislar.[5] The controlled jet is shown to return to axisymmetry at the longitudinal position $x/D = 3$, where the profiles I and II are superimposed.

The longitudinal evolution of the boundary layer momentum thickness and the volume flux through a plane normal to the jet axis, which are two characteristic quantities of the mean flow, are given in Figure 3. For the reference jet, the boundary layer momentum thickness (Figure 3(a)) is approximately a linear function of the longitudinal position, following the equation $\delta_\theta/D = 0.026(x/D + 0.14)$. The corresponding vorticity thickness roughly follows the law $\delta_\omega/D = 0.116(x/D + 0.16)$. This indicates that the ratio between these two estimations of the mixing layer thickness is about 4, which corresponds to the theoritical value derived from an hyperbolic tangent velocity profile. In its early development, the momentum thickness of the controlled jet is higher than that of the reference jet, but the longitudinal evolution follows a linear behavior with a slope lower than that of the reference case.

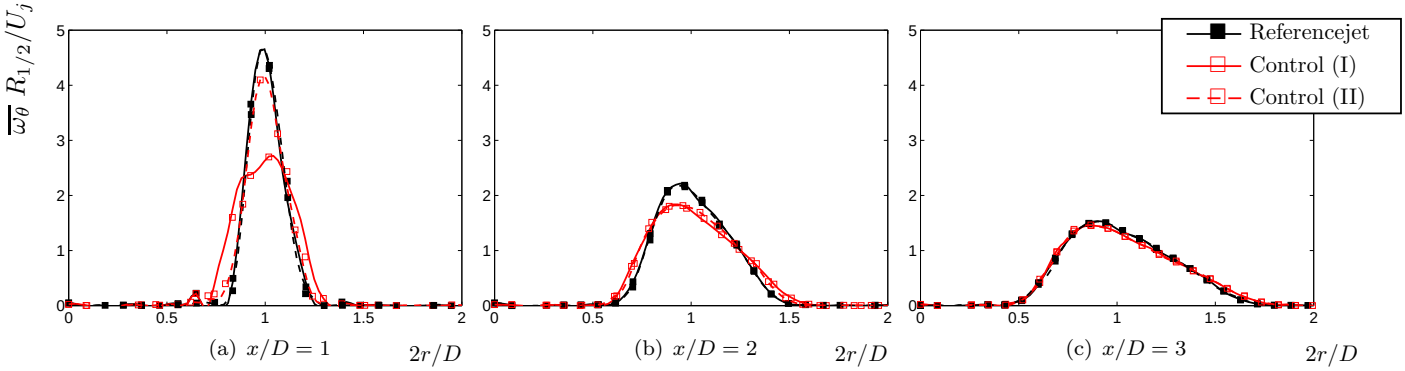

Figure 2. Radial profiles of the dimensionless mean azimuthal vorticity $\overline{\omega_\theta}\ R_{1/2}/U_j$, for three longitudinal locations of the measurement plane, with and without control. The profile obtained with the control and denoted I, respectively II, is extracted along the radius corresponding to the maximum, respectively minimum, mixing layer thickness.

The evolution of the volume flux Φ, represented in Figure 3(b) under the ratio with the initial volume flow Φ_0 estimated at the nozzle exit $x/D = 0$, follows the same trend. The volume flow is determined by the integration of the mean velocity - calculated over the transverse velocity field - over the radial coordinate. For the reference jet, the increasing rate of the volume flow with x/D is roughly constant and equal to 0.15. This value is consistent with the results given by Crow and Champagne,[13] Zaman and Raman,[14] and Liepmann and Gharib.[15] For the controlled jet, the evolution is still linear but the slope is now equal to 0.12; the controlled jet volume flux becomes lower than that of the reference jet at the longitudinal location $x/D = 3.5$. In the early development of the controlled jet, *e.g.* between $x/D = 1$ and $x/D = 3.5$, the volume flux through a plane normal to the jet axis is promoted by the control; the additional volume flux is shown to be located in the low-speed side of the jet, according to Figure 4. In this figure is represented the difference of axial mean velocity between the controlled jet and the reference jet, for four longitudinal positions of the measurements plane. These maps describe half of the jet. In the vincinity of the nozzle exit, typically for $x/D = 1$ or 2, a strong inhomogeneity is visible in the azimuthal direction, and the periodic (blue) blobs in the inner part of the jet correspond to the impingement location locally inducing a lack of axial velocity. In the low-speed side of the jet is obtained an almost homogeneous (red) area, corresponding to an excess velocity due to the control and provided by the entrainment of surrounding air. The velocity gradient through the jet mixing layer is lowered by the control, which is a result similar to those obtained with a flight effect[16] or in co-flow configurations, and explains the altered longitudinal evolution of the jet. Evolving more slowly because of the reduced shear through the mixing layer, the jet sees its potential core lengthened by the control, which can be derived from the excess velocity in the inner part of the jet at $x/D = 7$ (*c.f.* Figure 4(d)).

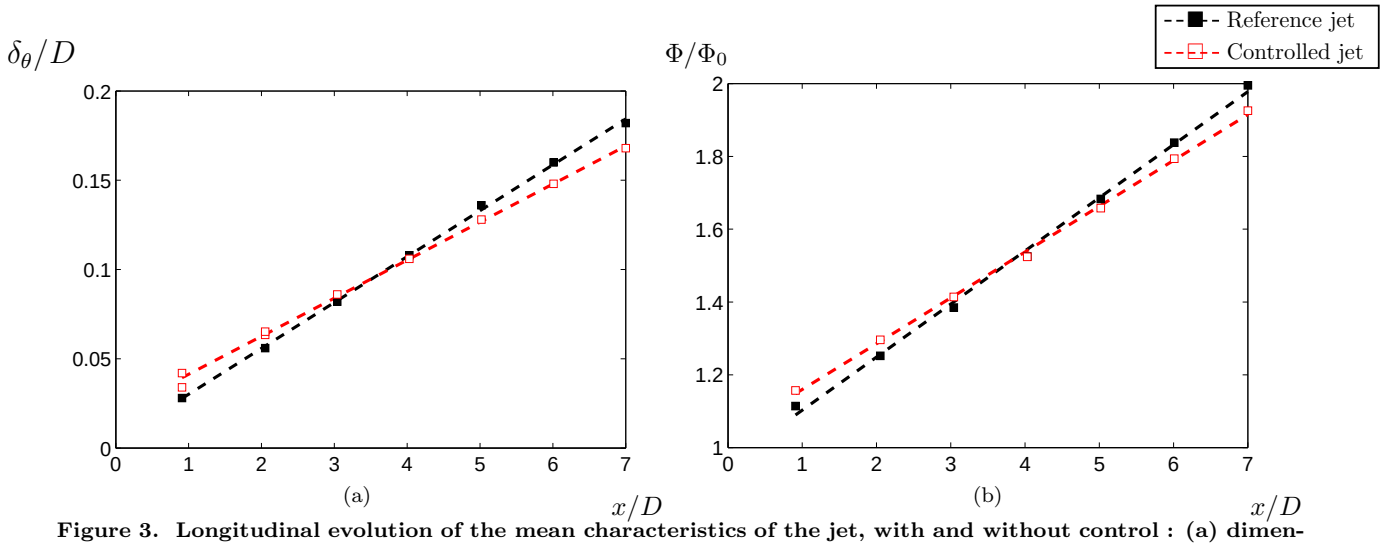

Figure 3. Longitudinal evolution of the mean characteristics of the jet, with and without control : (a) dimensionless momentum thickness δ_θ/D, (b) volume flux Φ related to the volume flux at the nozzle exit Φ_0.

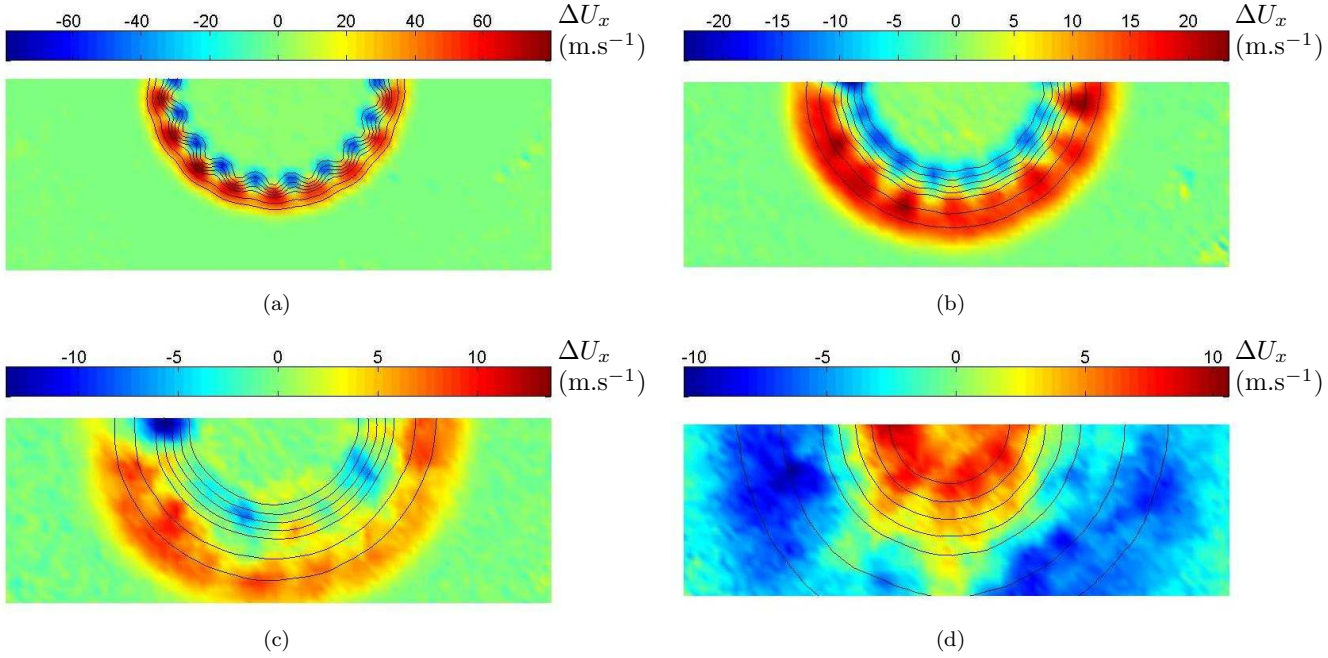

Figure 4. Difference of mean axial velocity between the controlled jet and the reference jet. The area in red (*respectively blue*) correspond to the flow region where the mean axial velocity is higher (*respectively lower*) with the control than in the reference case. The differences are calculated for the downstream location (a) $x/D =$ 1, (b) $x/D =$2, (c) $x/D =$3 and (d)$x/D =$ 7.

B. Effect of the mass flux per microjet

In the following, the effects of the mass flux injected by the microjets on the aerodynamic characteristics of the jet are examined. The mass flux of the control system is here described by the ratio r_m between the mass flux of one microjet and the mass flux of the main jet, adopting the same formalism as Castelain.[6] The mass flux per microjet is the parameter preferred to the total mass flux of the control, because the latter implicitly implies the total number of microjets n. For a given total mass flux of the control, the flow regime at the microjet exit can be varied by modifying the parameter n, and the transition from subsonic to supersonic regime can be obtained. The considered values of the parameter r_m are indicated in the Table 1. They describe the range adopted in the previous acoustic tests. As stated above, the microjet impingements modify the longitudinal evolution of the jet by changing the initial conditions of the jet development; for this particular reason, a detailed analysis of the flow field in the vincinity of the nozzle exit is proposed.

	$r_m^{(1)}$	$r_m^{(2)}$	$r_m^{(3)}$	$r_m^{(4)}$	$r_m^{(5)}$	$r_m^{(6)}$	$r_m^{(7)}$
$(\times 10^{-4})$	1.45	1.96	3.36	4.39	5.55	6.68	8.86

Table 1. Values of the parameter r_m.

The distribution of the turbulence intensity in the jet mixing layer at the longitudinal position $x/D = 1$ is given in Figure 5 for the turbulence intensity of the axial component of the velocity $u'_{x\ \mathrm{rms}}/U_j$ and in Figure 6 for the shear component of the Reynolds stress tensor $\sqrt{\overline{u'_x u'_r}}/U_j$. For the reference jet, the distribution of these quantities is remarkably axisymmetric and the maximum value of the turbulence intensity is in fair agreement with previous measurements on the same installation.[17] The control is seen to promote the corrugation of the jet mixing layer, with a depth increasing with r_m. This is illustrated in Figures 5 and 6 by the use of the white half-disk located in the potential core of the jet. The diameter of this geometrical form is unchanged between the different cases (a)-(h), and the inner part of the jet mixing layer is seen to get closer to the edge of this half-disk as the value of r_m increases. Moreover, the distribution of the maximum turbulence intensity is strongly dependent on the parameter r_m. For the values $r_m{}^{(1)}$ and $r_m{}^{(2)}$, the turbulence intensity level is not significantly altered by the control and remains roughly equal in the azimuthal direction. For $r_m \geq r_m{}^{(3)}$, the maximum turbulence intensity is higher than that of the reference jet, and the axisymmetry of the distribution is no longer obtained. Furthermore, the maximum turbulence intensity, located in the middle of the corrugated mixing layer for $r_m = r_m{}^{(3)}$ and $r_m = r_m{}^{(4)}$, progressively migrates to the low-speed side of the mixing layer on either side of the microjet impingements for higher values of r_m. The distribution of the shear component of stress tensor, in Figure 6, clearly highlights the loss of azimuthal homogeneity and the increase in the maximum value of the turbulence intensity for $r_m \geq r_m{}^{(5)}$. This characteristic value of r_m and the turbulence level enhancement in a region likely to radiate high-frequency noise owing to its typically lengthscales are fully consistent with the results of the previous acoustic study,[6] where high-frequency noise generation was induced by high values of r_m.

The return to axisymmetry is obtained at the longitudinal position $x/D = 3$ for the entire range of r_m. A mean profile of the turbulence intensity, derived from the maps in the transversal plane, can thus describe the distribution of the turbulence intensity, and in particular the value of its maximum. Figure 7 gives the evolution of the maxima of the turbulence intensity linked to the three components of the velocity and the maximum of the turbulent shear stress. These values are substracted to the corresponding quantities related to the reference jet, to illustrate the reduction provided by the control. A similar trend is noted for these four quantities : the turbulence reduction is almost tripled between $r_m{}^{(1)}$ and $r_m{}^{(3)}$, and remains almost constant up to $r_m{}^{(6)}$ before a new increase. This result is in excellent agreement with the corresponding conclusions of the acoustic study. The Sound Pressure Level (SPL) reductions with r_m, calculated[6,8] over the range [0:15kHz] are recalled in Figure 8 and exhibit a behavior highly correlated to the aerodynamic results of Figure 7. The frequency range [0:15kHz] is chosen for the SPL calculation to exclude high-frequency noise considerations, considering as stated before that high-frequency noise generation comes from the early stages of the jet development typically located upstream the longitudinal position $x/D = 3$.

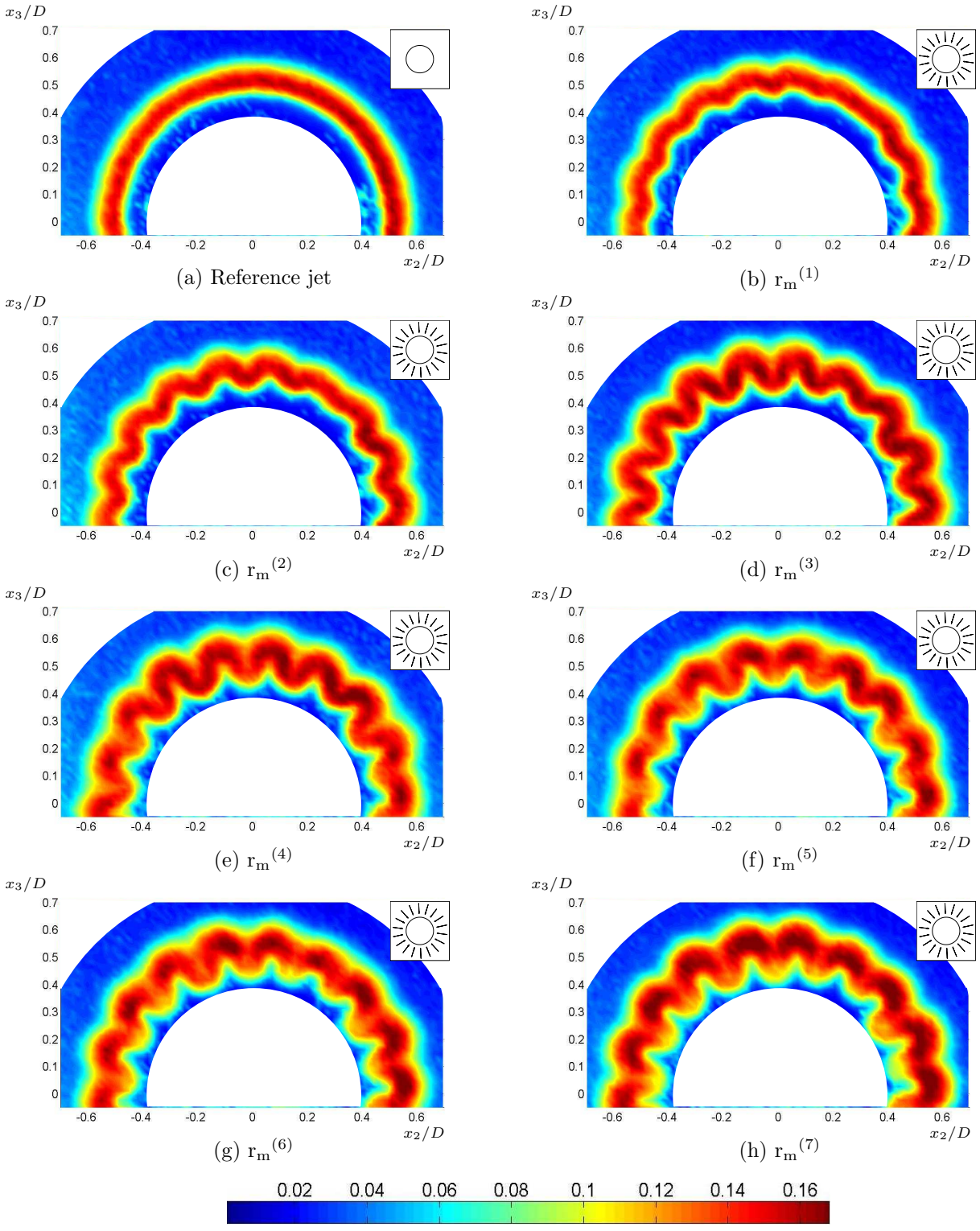

Figure 5. Maps of $u'_{x\ \mathrm{rms}}/U_j$ for the tested values of the mass flux ratio r_m. The reference jet case (a) is compared to the results obtained with the values of r_m listed in Table 1 ; the sketch at the top-right of each map indicates the azimuthal distribution of the microjets. Longitudinal position: $x/D = 1$

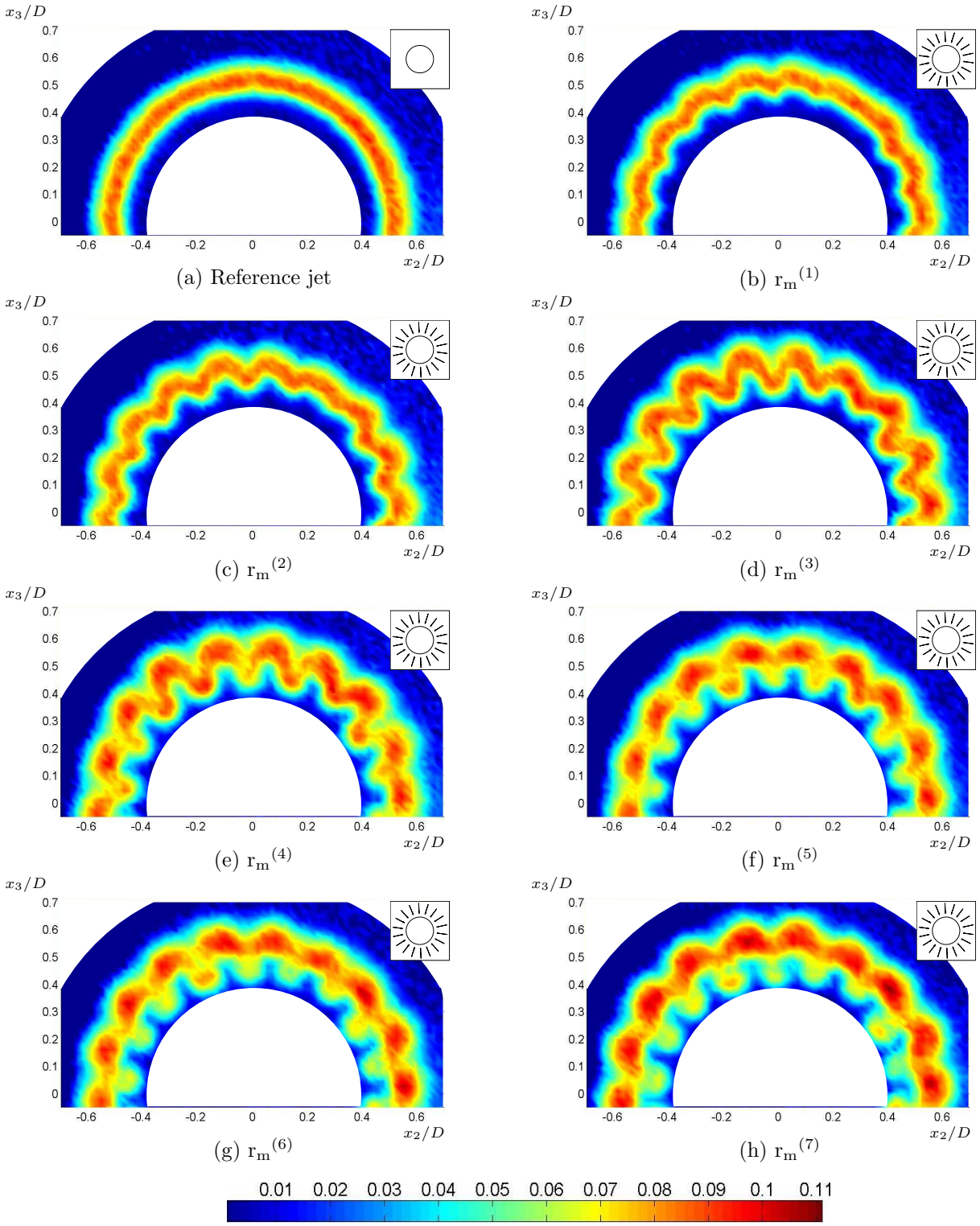

Figure 6. Maps of $\overline{u'_x u'_r}^{1/2}/U_j$ for the tested values of the mass flux ratio r_m. The reference jet case (a) is compared to the results obtained with the values of r_m listed in Table 1 ; the sketch at the top-right of each map indicates the azimuthal distribution of the microjets. Longitudinal position: $x/D = 1$

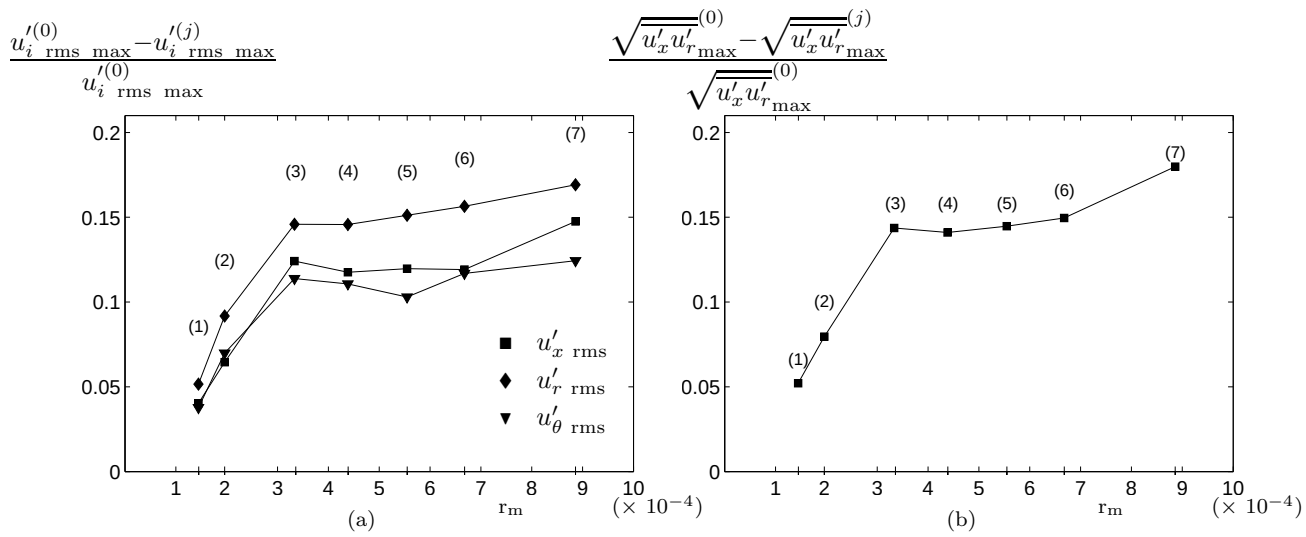

Figure 7. Turbulence reduction with the mass flux ratio r_m. The turbulence reduction, calculated with the maximum of the rms value of the three components of the velocity (a) or the shear stress (b), is given for the values of $r_m^{(j)}$ reported in Table 1 and expressed as a percentage of the reference value (superscript $^{(0)}$). Longitudinal position: $x/D = 3$

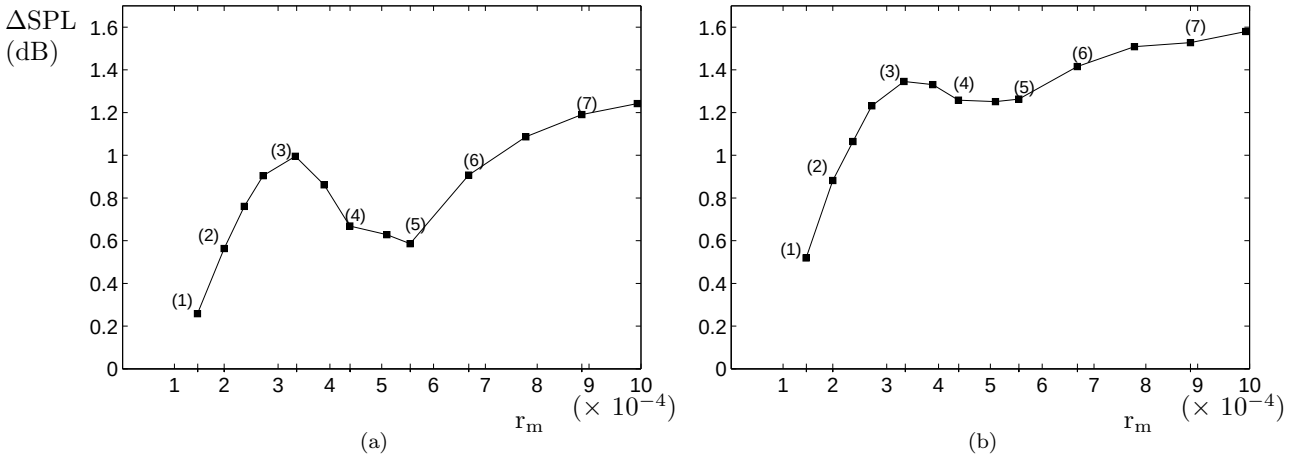

Figure 8. Sound Pressure Level reduction with the mass flux ratio r_m. The noise level is determined in the frequency range [0:15 kHz] for the values of $r_m^{(j)}$ reported in Table 1, at the angle (a) $\phi = 30°$ and (b) $\phi = 90°$ with respect to the downstream jet axis.

C. Effect of the number of microjets

In this section the parameters of the microjet system are constant, at the exception of the number of microjets n, varied from 3 to 36 by maintaining an axisymmetric layout. The mass flus ratio r_m is set to 2.7 10^{-4}, and corresponds to a configuration avoiding any acoustic penalty in the high-frequency domain;[6,8] the configuration with 36 microjets also exhibits a slight high-frequency noise reduction with respect to the reference case. The examination of the turbulence parameter in the early stages of the jet development, and typically at $x/D = 1$, seems consequently crucial to put some light on these acoustic results. The distribution of the turbulence intensity corresponding to the axial velocity and the shear stress are given in Figures 9 and 10. It appears that, for a sufficiently low number of microjets (typically $n \leq 12$), an unperturbed area remains at $x/D = 1$ between two consecutive microjet impingements; the turbulence level

and its distribution in the jet mixing layer correspond to those obtained in the reference case. Identical patterns of turbulence level distribution are obtained with the configuration implying $n = 6$ or $n = 12$ microjets - as illustrated by the microjet located on top of each figures - which denotes the independence of consecutive microjets. For example, the edge of the white half-disk, used to help the visual estimation of the indentation due to the impingements of microjet, remains exactly at the inner limit of the corrugated mixing layer for $n \leq 12$. Increasing the number of microjets results in promoting the interaction between consecutive microjets, because the azimuthal separation between the microjets become small with respect to the spatial extent of the perturbations induced in the jet mixing layer. This interaction probably already occurs for $n = 18$, as no unperturbed mixing layer is left between two consecutive impingements. A spatial frequency of the perturbations in the azimuthal direction can be easily derived from the patterns of Figures 9(a)-(e) and 10(a)-(e), and correspond to the azimuthal frequency of the microjets impingement. Doubling the number of microjets (*i.e.* $n = 36$, in Figures 9(g) and 10(g)) provides aerodynamic results in which a particular spatial frequency of the perturbations in the azimuthal direction cannot be determined. The maximum turbulence level is significantly lower than that of the reference jet, which is consistent with the corresponding reduction of the noise emitted in the high-frequency domain, and the distribution of the turbulence intensity is almost homogeneous in the azimuthal direction - the small azimuthal inhomogeneities being attributed to the slight misalignement of some microjets. The configuration with $n = 24$ microjets stands for a mixed configuration with paired microjets. The angular separation between the two microjets of each pair corresponds to the angular separation of the $n = 36$ configuration and the angular separation between the two pairs of microjets corresponds to the angular separation of the $n = 18$ configuration. The spatial frequency of the flow modifications in the azimuthal direction corresponds to that of the twelve paired microjets.

Furthermore, as recalled in Figure 11, the maximum SPL noise reduction is not obtained for the maximum number of microjets, and an optimum number of microjets, taking the value $n = 18$ in our case, exists. In Figure 12, the maxima of turbulence at the longitudinal location $x/D = 3$ are given as a function of the number of microjets n. The turbulence reduction for the three components of the velocity and for the shear stress is shown to increase with n roughly up to 12%, obtained for $n = 18$, and diminish for higher values of n. This trend is very close to that obtained from the acoustic results of Figure 11, and this correlation between the aerodynamic parameters in the $x/D = 3$ and the acoustic far-field measurements is similar to the one noticed for the study of the effect of r_m.

D. Effect of the microjets layout

The previous acoustic study[6] considered the influence of the microjets layout on jet noise reduction, for a given number of microjets n. This study thus first involved a configuration with $n = 18$ axisymmetrically-distributed microjets, which corresponds to that of the section B, and secondly a configuration with $n = 9$ microjets distributed in one half of the main jet, which represents "half" of the first configuration. It was demonstrated that the noise reduction obtained with the latter is half that promoted by the axisymmetric distribution, the cost of the control being also divided by two. This confirms the conclusions obtained in section C about the cumulative effect of the microjets, linked to their relative independency for sufficiently low values of n. Considering these acoustic results, the aerodynamic effect of each microjet could consequently be isolated, and the persistency of this effect in the jet development could be characterized. This leads to the testing of the aerodynamic modifications of the flow induced by the $n = 9$ asymmetric and $n = 18$ symmetric configurations. The turbulence intensity distribution in the $x/D = 1$ and $x/D = 3$ planes are given in Figure 13, the controlled side of the jet being its right-half in the case of the asymmetric configuration. We notice that, at the $x/D = 1$ longitudinal position (left column of the Figure 13), the pattern of the corrugation induced by the four microjets whose impingements are contained in the cameras field of view and the associated turbulence level are almost independent of the controlled configuration, be it the $n = 9$ asymmetric or the $n = 18$ symmetric one. The only difference on the right side of the jet between these two controlled cases is the side effect obtained with the $n = 9$ asymmetric configuration (top of the figure). At the longitudinal position $x/D = 3$ (right column of the Figure 13), the controlled jet has returned to axisymmetry yet, and the turbulence level are homogeneous in the azimuthal direction for the axisymmetric configurations, *i.e.* the reference jet and the $n = 18$ axisymmetric configuration. Any asymmetry of the control remains at least until the longitudinal position $x/D = 3$, as denoted by the results obtained with the $n = 9$ asymmetric configuration. The right side of the jet, facing the microjets, sees an homogeneous distribution of the turbulence intensity, whose maximum value is identical to that obtained with the $n = 18$

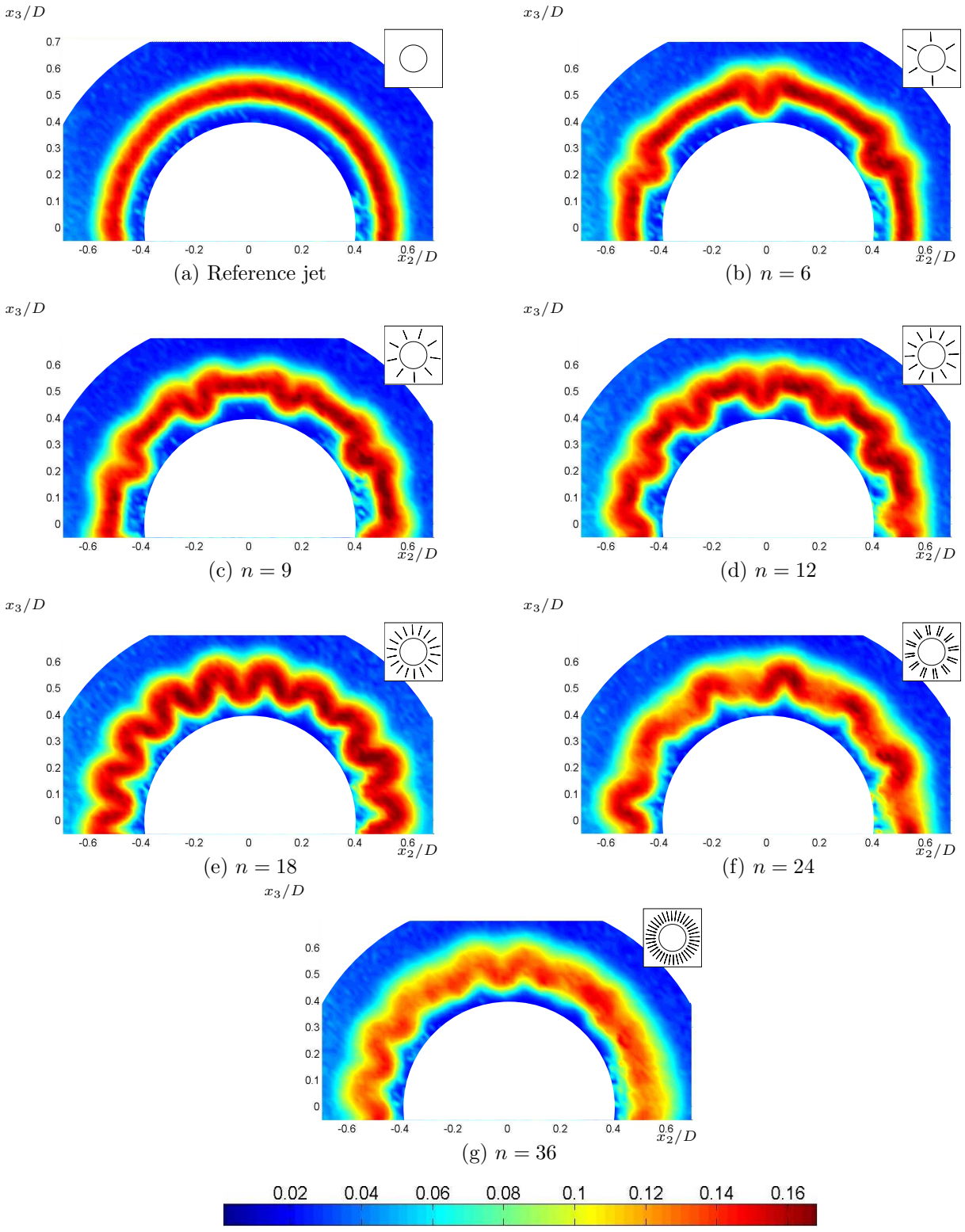

Figure 9. Maps of $u'_{x\ \mathrm{rms}}/U_j$ for the tested values of the number of microjets n. The reference jet case (a) is compared to the configurations implying 6 (b), 9 (c), 12 (d), 18 (e), 24 (f) and 36 (g) microjets; the sketch at the top-right of each map indicates the azimuthal distribution of the microjets. Longitudinal position: $x/D = 1$

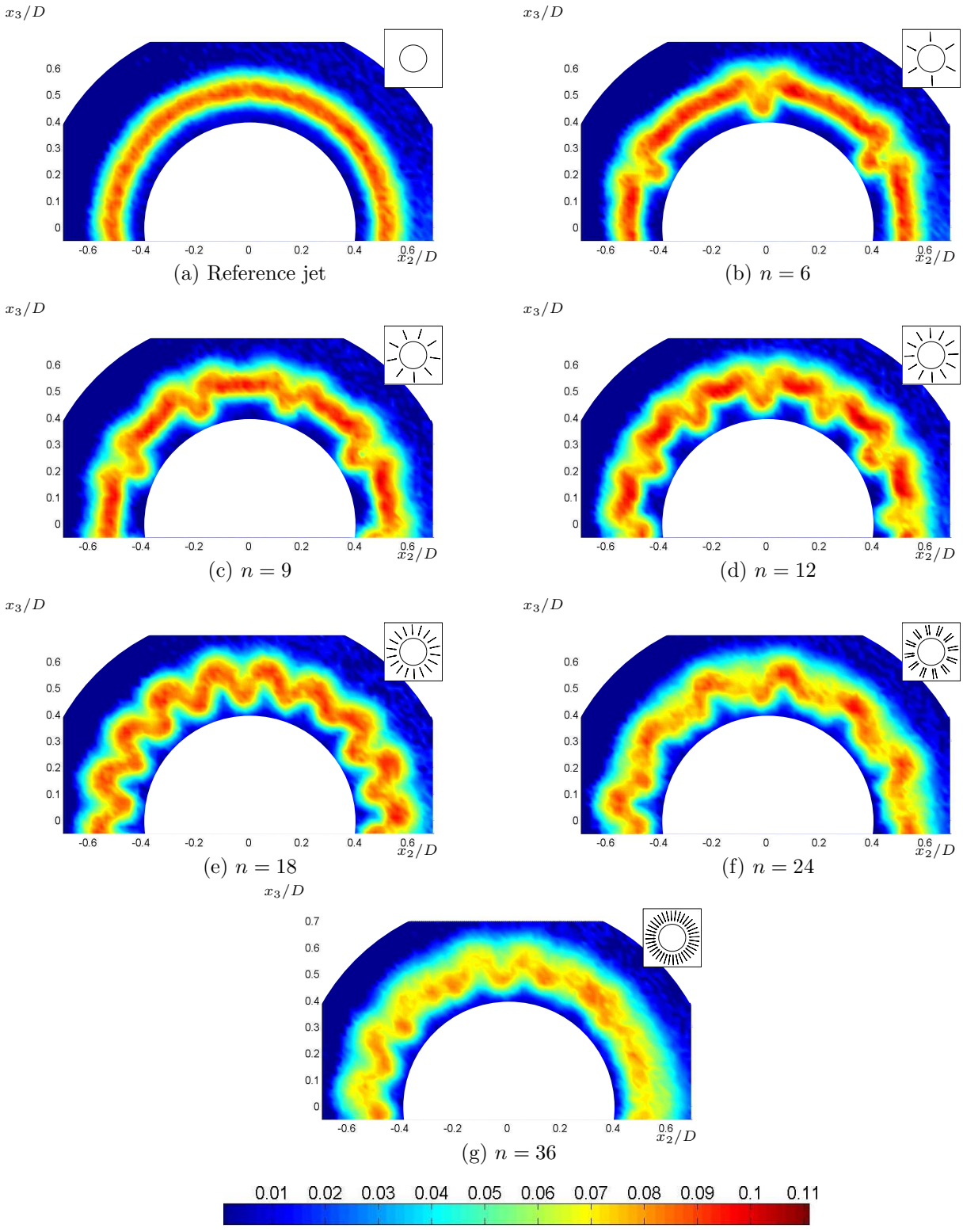

Figure 10. Maps of $\overline{u'_x u'_r}^{1/2}/U_j$ for the tested values of the number of microjets n. The reference jet case (a) is compared to the configurations implying 6 (b), 9 (c), 12 (d), 18 (e), 24 (f) and 36 (g) microjets; the sketch at the top-right of each map indicates the azimuthal distribution of the microjets. Longitudinal position: $x/D = 1$

axisymmetric configuration, as reported in the Table 2. The distribution of the turbulence intensity in the uncontrolled side of the jet is also homogeneous, but its maximum level corresponds then to that of the reference jet. This tends to indicate that the reduction of turbulence induced by the microjets is convected downstream without any azimuthal diffusion until $x/D = 3$.

	Reference jet Fig.13(a)	$n = 9$ half circumference Fig.13(b)	$n = 18$ axisymmetric Fig.13(c)
$\max(u'_{x\ \mathrm{rms}}/U_j)$ right-half of the map	0.160	0.139	0.140
$\max(u'_{x\ \mathrm{rms}}/U_j)$ left-half of the map	0.161	0.160	0.139

Table 2. Maximum value of the turbulence intensity related to the axial component of the velocity, resulting from the average on the right-half and the left-half of Figure 13 for different microjets layouts. The axisymmetric configurations exhibit identical mean values for the two averagings. Longitudinal position : $x/D = 3$

IV. Conclusions

An aerodynamic study of the effect of microjets on a high-subsonic high-Reynolds jet is performed and are interpreted in the light of previous acoustic results. These measurements relies on Stereoscopic Particle Image Velocimetry in planes normal to the jet axis. The distribution of the turbulence intensity in these planes exhibits a corrugation of the main jet flow, which, in the case of an axisymmetric configuration of the microjets system, returns to homogeneity in the azimuthal direction for a longitudinal distance comprised between two and three times the nozzle diameter downstream the nozzle exit. Three parameters of the microjets system are varied : the outgoing mass flux per microjet, the number of microjets and their layout in the azimuth of the main jet. The aerodynamic results indicate a strong correlation between the maximum level of turbulence just behind the nozzle exit (characterized here one nozzle diameter downstream the nozzle exit) and the high-frequency noise, previously shown to potentially balance the acoustic benefits obtained for lower frequencies. The maximum level of turbulence measured downstream (here three nozzle diameters downstream the nozzle exit) is also highly correlated to the jet noise reduction, which is highlighted by the similar evolution of these two quantities regarding the mass flux per microjet and the number of microjets. For low values of the number of microjets, the microjets are shown to act independently, and their contributions to the turbulence reduction are retrieved far downstream the impinging point without any noticeable azimuthal diffusion.

References

[1]Simonich, J. and Narayanan, S., "Aeroacoustic characterization, noise reduction and dimensional scaling effects of high subsonic jets," *AIAA j.*, Vol. 39, No. 11, 2001, pp. 2062–2069.

[2]Zaman, K., "Effects of delta tabs on mixing and axis switching in jets from axisymmetric nozzles," *AIAA paper 1994-0186*, 1994.

[3]Zaman, K., "Spreading characteristics of compressible jets from nozzles of various geometries," *J. Fluid Mech.*, Vol. 383, 1999, pp. 197–228.

[4]Arakeri, V. and Krothapalli, A., "On the use of microjets to suppress turbulence in a Mach 0.9 axisymmetric jet," *J. Fluid Mech.*, Vol. 490, 2003, pp. 75–98.

[5]Alkislar, M., Krothapalli, A., Lourenco, L., and Butler, G., "The effect of streamwise vorticity on the aeroacoustics of Mach 0.9 axisymmetric jet," *AIAA paper 2005-3045.*, 2005.

[6]Castelain, T., Béra, J., Sunyach, M., and Juvé, D., "Effect of microjets on a high-subsonic jet. Parametric study of far-field noise reduction." *AIAA paper 2006-2705*, 2006.

[7]Castelain, T., Béra, J., and Sunyach, M., "Noise reduction of a Mach 0.7-0.9 jet by impinging microjets," *C.R.Mécanique*, Vol. 334, 2006, pp. 98–104.

[8]Castelain, T., *Contrôle de jet par microjets impactants. Mesure de bruit et analyse aérodynamique.*, Ph.D. thesis, Ecole Centrale de Lyon, 2006.

[9]Raffel, M., Willert, C., and Kompenhans, J., *Particle image velocimetry, a practical guide*, Springer, 1988.

[10]Melling, A., "Tracer particles and seeding for particle image velocimetry," *Meas. Sci. Technol.*, Vol. 8, 1997, pp. 1406–1416.

[11]Scarano, F. and Riethmuller, M., "Iterative multigrid approach in PIV image processing with discrete window offset," *Exp.Fluids.*, Vol. 26, 1999, pp. 513–523.

[12]Wieneke, B., "Stereo-PIV using self-calibration on particle images," *Exp.Fluids*, Vol. 39, 2005, pp. 267–280.

[13]Crow, S. and Champagne, F., "Orderly structure in jet turbulence," *J. Fluid Mech.*, Vol. 48, 1971, pp. 547–591.

[14]Zaman, K. and Raman, G., "Reversal in spreading of a tabbed circular jet under controlled excitation," *Phys. Fluids*, Vol. 9(12), 1997, pp. 3733–3741.

[15]Liepmann, D. and Gharib, M., "The role of streamwise vorticity in the near-field entrainemen of round jets," *J. Fluid. Mech.*, Vol. 245, 1992, pp. 643–668.

[16]Morris, P., "Turbulence measurements in subsonic and supersonic axisymmtric jets in a parallel stream," *AIAA j.*, Vol. 14(10), 1976, pp. 1468–1475.

[17]Fleury, V., *Superdiretivité, bruit d'apariement et autres contributions au bruit de jet subsonique*, Ph.D. thesis, These de doctorat, École Centrale de Lyon, 2006.

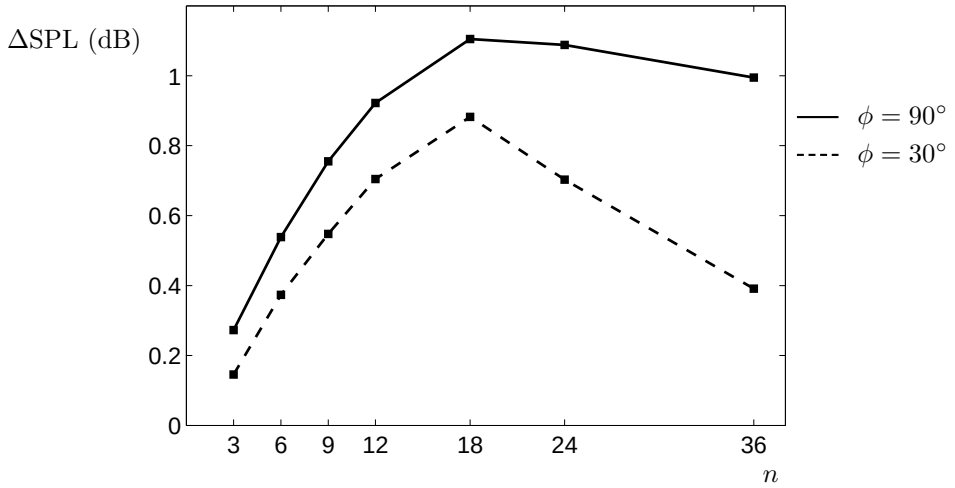

Figure 11. Evolution of the Sound Pressure Level reduction, calculated over the frequency range [0:35kHz], with the number of microjets n, for two angles of directivity ϕ.

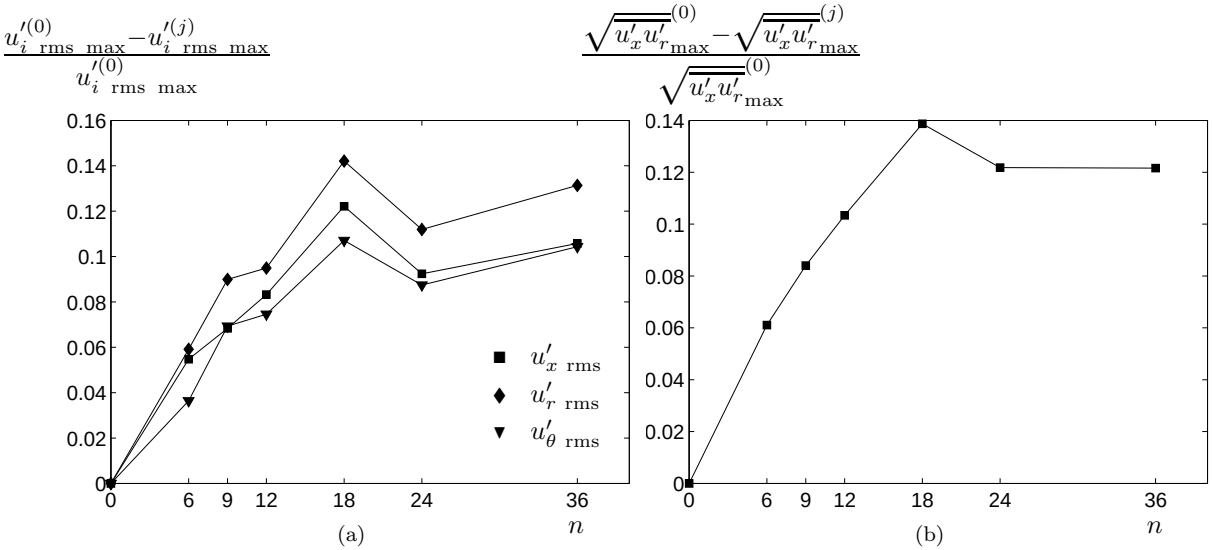

Figure 12. Turbulence reduction with the number of microjets n. The turbulence reduction, calculated with the maximum of the rms value of the three components of the velocity (a) or the shear stress (b), is given for the values of n between 3 and 36 and expressed as a percentage of the reference value (superscript $^{(0)}$). Longitudinal position: $x/D = 3$

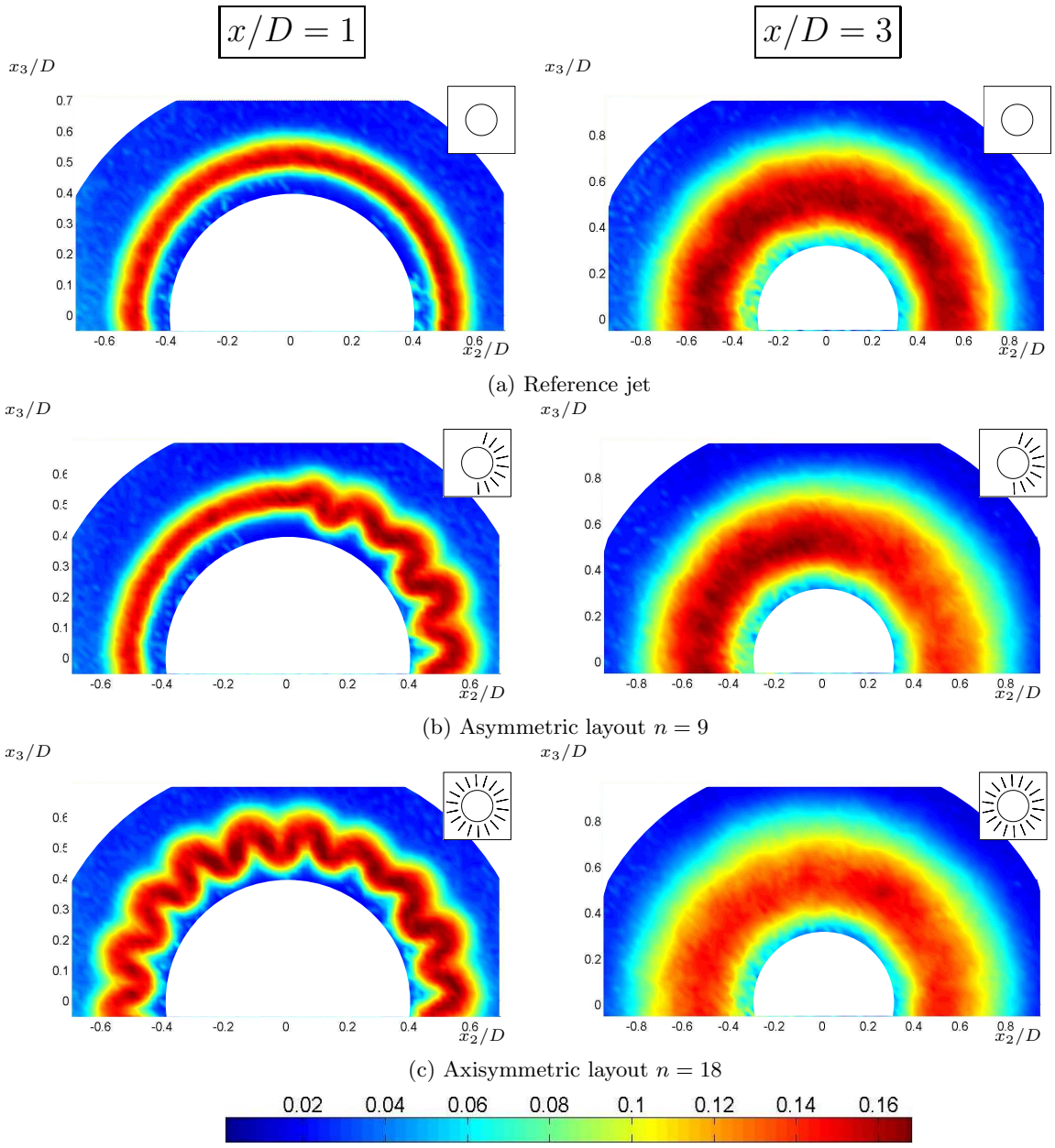

Figure 13. Maps of $u'_{x\ \mathrm{rms}}/U_j$ for the reference jet (a), the control case with $n = 9$ microjets distributed one one half of the jet (b), and for the axisymmetric configuration with $n = 18$ microjets. The longitudinal position is $x/D = 1$ (left column) and $x/D = 3$ (right column)